ELSEVIER

Cement & Concrete Composites 24 (2002) 457–465

Cement & Concrete Composites

www.elsevier.com/locate/cemconcomp

Impedance spectroscopy of fiber-reinforced cement composites

T.O. Mason *, M.A. Campo, A.D. Hixson, L.Y. Woo

Department of Materials Science and Engineering, Center for Advanced Cement-Based Materials, Northwestern University, 2225 North Campus Drive, Evanston, IL 60208-4400, USA

Abstract

The addition of chopped conductive fibers to cement matrices results in a characteristic "dual-arc" electrical impedance spectrum below the percolation threshold. This behavior can be explained on the basis of a "frequency-switchable fiber coating" model, in which a "coating" (e.g., passive oxide film on steel or charge transfer resistance/double layer on other conductors) insulates the fibers at DC and low AC frequencies, but is shorted out at higher frequencies, where the fibers become short-circuit paths in the composite microstructure. The present work investigates various factors governing the impedance spectra of fiber-reinforced cement composites – fiber aspect ratio, fiber volume fraction, fiber orientation (relative to field direction), and fiber shape. The "gamma" factor (ratio of the low frequency arc diameter to DC resistance) is a useful parameter to characterize the microstructure–property relationships of fiber-reinforced composites.

Keywords: Electrical impedance spectroscopy; Carbon fiber composites; Steel fiber composites

1. Introduction

The role of fibers in the strengthening and toughening of otherwise brittle matrices is clearly established and the underlying mechanisms are well understood [1]. In contrast, the role of fibers in determining the electrical properties of composites is not as clearly established, nor are the underlying microstructure–property relationships as well developed. The present study was undertaken to investigate the AC impedance response of cement-based composites incorporating short conductive fibers, to evaluate the applicability of the recently proposed "frequency-switchable fiber coating" model for AC impedance properties [2,3], and to study the influence of various factors (fiber aspect ratio, fiber volume fraction, fiber orientation, and fiber shape) on the resulting impedance spectra.

It is widely accepted that the DC electrical properties are sensitive to the microstructure and strain-induced changes in microstructure in fiber-reinforced composites. For example, the DC conductivity of unidirectional composites in the fiber direction has been employed to assess fiber content [4] and also to assess damage in static and dynamic loading [5–7]. Below the percolation threshold (i.e., no continuous fiber conduction path) discontinuous conductive fibers can still affect the DC electrical properties of composites. For example, Chung and co-workers demonstrated strain-induced DC resistance changes in polymer-matrix [8], ceramic-matrix [9], and concrete-matrix composites [10,11] incorporating short conductive fibers. Chung discussed the potential for "self-monitoring" of such composites, with respect to deformation and damage mechanisms, via electrical property measurements [7].

The AC electrical properties of composites have received less attention than the DC properties. Gu et al. [12] made impedance measurements of cement-matrix composites with wollastonite micro-fibers. Because the fibers were insulating, only one impedance arc was obtained. Gerhardt [13] reported Nyquist plots ($-Z_{\text{imaginary}}$ vs. Z_{real}) for hot-pressed mullite-matrix composites with 10% SiC whiskers. Two arcs were obtained, with their relative sizes varying with the direction of applied field (perpendicular vs. parallel to the hot-pressing direction). Similarly, Wang et al. [14] obtained dual-arc Nyquist plots for extruded/hot-pressed silicon nitride-matrix composites with 20 wt% SiC whiskers. Again, the relative size of the two arcs varied with the direction of applied field; the low frequency arc disappeared when the field was applied parallel to the hot-pressing direction

* Corresponding author. Fax: +1-847-491-7820.
E-mail address: t-mason@northwestern.edu (T.O. Mason).

0958-9465/02/$ - see front matter © 2002 Published by Elsevier Science Ltd.
PII: S0958-9465(01)00077-4

(i.e., perpendicular to the fibers). Ford et al. [15] reported dual-arc Nyquist plots for cement composites with 1 vol% steel fibers, vs. only one arc without the fibers, and referred to the low frequency composite arc as the "fiber-induced arc".

Recently our laboratory published two studies of conductive fiber-reinforced cement-matrix composites. The first study [2] confirmed the dual-arc impedance response of steel fiber-reinforced cement paste composites, and developed a "fiber-switchable coating model" to explain this behavior. This model was based on a single fiber simulator (with tap water as the "matrix") and was confirmed by pixel-based computer simulations. At low frequencies, the passive oxide film on the steel fibers effectively insulates them electrically from the matrix. At small volume fractions, their presence has virtually no effect on the DC and low AC frequency properties, which are governed exclusively by the cement paste matrix. As frequency increases, however, displacement currents through the thin oxide film capacitance short out the coating, whereupon the fibers act as short circuits for current flow. This results in subdivision of the single bulk arc (without fibers) into two arcs (with fibers). It should be stressed that both arcs are "fiber-induced", i.e., they are part of the overall impedance spectrum for the composite.

The second study [3] reported a preliminary investigation of fiber orientation effects on AC impedance spectra. Again, the single fiber simulator was employed. When field was applied in the direction of the fiber axis the greatest degree of bulk arc subdivision was obtained, i.e., the low frequency arc was at its largest. On the other hand, with field applied perpendicular to the fiber axis no low frequency arc was obtained; the behavior was virtually indistinguishable from the case with no fiber present. This was explained in that only the fiber diameter (negligibly small as compared with the fiber length) was available for short-circuit current flow at high frequencies.

The present work investigated composites incorporating fibers with and without passive oxide films (steel vs. carbon). It also made a more thorough investigation of fiber-based microstructural variables, including fiber aspect ratio, fiber volume fraction, fiber orientation (vs. applied field direction) and fiber shape. Both actual composite measurements and single fiber simulator experiments were performed.

2. Experimental procedures

Fiber-reinforced composites with 1 wt% of fibers were prepared from type I ordinary portland cement (OPC) with a water-to-cement ratio of 0.4 by weight. Steel fibers (2 mm long, 30 μm diameter) or carbon fibers (18 mm *initial* length, 18 μm diameter) were dry-mixed with the cement by hand for 1 min. Water was added, followed by hand-mixing for approximately 3 min. The mixture was then blended on high speed in a commercial blender for approximately 2 min to achieve homogenization. This significantly reduced the carbon fiber length, as described below. Plain OPC specimens (without fibers) were similarly mixed. Specimens were cast in rectangular polycarbonate containers (25 mm × 25 mm × 100 mm) with stainless steel electrodes (20 mm × 30 mm × 0.5 mm) cast in place approximately 5 mm from each end, corresponding to an inter-electrode spacing of 90 mm. All samples were stored in a 100% RH chamber during curing. In a separate study [16], nitric acid was used to dissolve away the matrix cement of a carbon fiber-reinforced composite (0.5 vol% fibers) made from the identical fibers employed in the current study. Optical microscopy on the residual fibers showed a distribution of fiber lengths (0.1–2.3 mm), with the median length close to 1 mm.

Single wire/fiber simulation studies were carried out in tap water, which roughly approximates the resistivity/dielectric constant of mature cement paste [2,3]. Three different polymer chambers were used for these experiments. One was the same size as used for the composite experiments (25 mm × 25 mm × 100 mm), with electrodes placed 90 mm apart (5 mm from each end). The other was larger (125 mm × 240 mm × 330 mm), and could accommodate longer "fibers" with dumbbell and hooked-ends whose radial dimensions were substantial when compared to the 25 mm cross-section of the smaller chamber. It could also accommodate fiber rotation studies. Its electrodes (approximately 100 mm × 100 mm × 1 mm) were positioned at either end of the chamber (290 mm apart). A support system made from polymer mesh was used to suspend fibers in water within each chamber. Impedance measurements with and without the mesh showed it had negligible effect on the impedance spectra. A protractor, suspended on the plastic mesh beneath the wires, was used to vary and measure the orientation of wires/fibers in the large chamber relative to the direction of applied field. The third polymer chamber consisted of a 2000 ml graduated cylinder with two 150 mm long steel rods (6.4 mm diameter). One rod was secured vertically on a piece of polycarbonate placed at the bottom of the cylinder. The cylinder was filled with water to an appropriate level with the second steel rod lowered from a ring stand into the top of the cylinder, in line with the lower rod. The separation of the two rods was varied, always maintaining the submersion depth of the upper rod at 150 mm.

Impedance measurements were carried out using a personal computer-controlled frequency response ana-

lyzer, either the Solartron 1260 with Z60 control software (Solartron Instruments, Hampshire, UK) or the Hewlett-Packard 4192A (Hewlett-Packard, Palo Alto, CA) with control software written in our laboratory. Frequency was swept from the 10 MHz range to the Hz range with data collected at intervals of 20 points per decade at an excitation amplitude of 1 V. In certain cases frequency was swept as low as 5 mHz (using the Solartron 1260) to get a better idea of the impedance arc associated with the measuring electrodes. For these measurements a low excitation amplitude (50 mV) was employed. In certain instances, data manipulation was accomplished using the commercially available software package, "Equivalent Circuit" [17].

To confirm the DC resistance of the composite specimens, four-point measurements were also performed. The specimens were removed from their molds and two thin bands (~1 mm wide) of silver paint were placed around each sample at positions approximately 1/3 of the sample length from either end. A variable voltage DC power supply (1–150 V) was used to provide current through the embedded steel electrodes and the resulting voltage drop was measured between the two silver paint electrodes. These measurements were carried out as quickly as possible to minimize the deleterious effects of current flow and/or joule heating [18]. In every case ohmic behavior was observed.

3. Results and discussion

3.1. Impedance spectra of composites and simulator results

Fig. 1 shows Nyquist plots at 3 days of hydration for 0.4 w/c ratio OPC composites without and with either 1 wt% steel fibers or 1 wt% carbon fibers. Also shown are the four-point DC resistance values, corrected for the difference in inter-electrode spacings in DC vs. AC measurements. In each case there is good agreement between the DC resistance and the cusp between the electrode arc (to the right) and the bulk features (to the left of the DC resistance). This was interpreted as indicating that both composites are below their percolation thresholds for the conducting fibers. These observations are also in agreement with prior studies [2,3] with respect to negligible shift in DC resistivity (conductivity) and subdivision of the bulk arc into two arcs upon the addition of fibers.

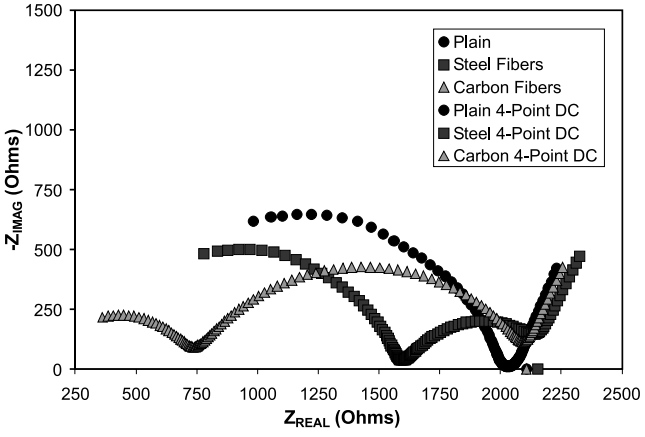

Fig. 1. Nyquist plots for $w/c = 0.4$ OPC matrices at 3 days of hydration without and with 1 wt% additions of either steel or carbon fibers. Four-point DC resistances are shown for comparison.

Fig. 2(a) displays the raw data for a single wire in the simulator of the same size as for the OPC results in Fig. 1. In this case the wire was carbon (graphite) 60 mm long by 0.5 mm diameter, and the electrodes were aluminum. This selection of materials gave the best separation of the low frequency bulk arc and the electrode arc. When identical materials were used for "fiber" and electrode, their arcs were often strongly convoluted. By taking impedance data to much lower frequencies (5 mHz) we were able to fit the spectra and remove the electrode arc, leading to the results in Fig. 2(b). This plot shows the "bulk only" (electrode-removed) features with and without the carbon "fiber". The slight discontinuity in the bulk arc(s) near the cusp frequency in Fig. 2(a) is attributable to the low excitation amplitude used for these experiments; the discontinuity disappears when larger amplitudes are employed. The general features – negligible influence of the "fiber" on DC resistance and subdivision of the single bulk arc (without the fiber) into two arcs (with the fiber) in Fig. 2(b) – are consistent with the experimental results for the actual composites in Fig. 1.

We have previously explained this dual-arc behavior with the "frequency-switchable coating" model [2,3]. The single fiber representation and corresponding equivalent circuit are shown in Figs. 3(a) and (b), respectively. For the sake of simplicity, the electrode components have not been shown. The upper path in Fig. 3(b) represents the bulk cement paste (R_b, C_b) and the lower path represents the short-circuit "fiber" path. In this path, the switch represents the "coating" elements (R_{coat}, C_{coat}). For steel fibers, R_{coat} consists primarily of the passive oxide film resistance, which can be quite large [15]. Therefore, at DC and low AC frequencies this film completely insulates each fiber from the surrounding matrix. This is why the DC resistance changes negligibly upon small (sub-percolation threshold) additions of steel fibers (see Fig. 1), and current flow is relatively unperturbed by the wire being present (see the dashed lines in Fig. 3(a)). In the case of carbon and other conductors, which do not form an oxide coating, a polarization layer (charge transfer resistance/double

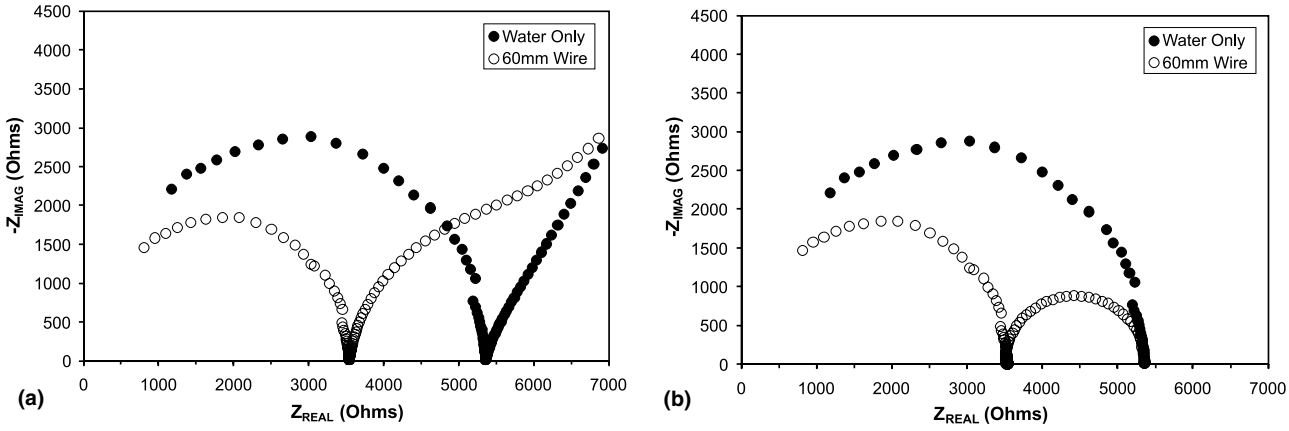

Fig. 2. Raw (a) and modified (b) Nyquist plots for a single graphite rod (60 mm long, 0.5 mm diameter) in tap water between aluminum measurement electrodes. In (b) the electrode arc has been removed mathematically.

layer capacitance) nevertheless forms to accomplish a similar result.

As frequency increases, however, displacement currents through the thin coating capacitor (C_{coat}) act to short out R_{coat}, "turning on" the switch in the lower path of Fig. 3(b). The current flow is now as shown by the solid lines in Fig. 3(a). Most of the bulk, except for the outer bulk regions (R_{ob}, C_{ob}) between the wire tips and the electrodes, becomes bypassed. In addition, however, there is current-bunching to the wire/fiber tips, leading to spreading resistance contributions to the lower path resistance (R_{sp}, C_{sp}). Pixel-based computer modeling in our prior study [2] clearly showed the state of current flow. At DC the wire/fiber was dark (no current was flowing in it). At the "cusp frequency" (between the two bulk arcs), the wire appeared bright (heavy current flow), as were the matrix zones near the tips of the wire due to local current-bunching. The matrix surrounding the middle of the wire, on the other hand, was dark (little current flow) consistent with current bypassing these regions via the less resistive wire/fiber path.

3.2. The influence of fiber aspect ratio

Aspect ratio is defined as the length-to-diameter ratio of the fibers employed. Wire diameter plays a significant role in determining spreading resistance at the fiber/wire tips. For a wire just touching the surface of a conductive medium, the spreading resistance (R_{sp}) is given by [19]:

$$R_{sp} = (4\sigma a)^{-1}, \tag{1}$$

where σ is the conductivity of the medium and a is the radius of the wire. As the wire becomes submerged in the

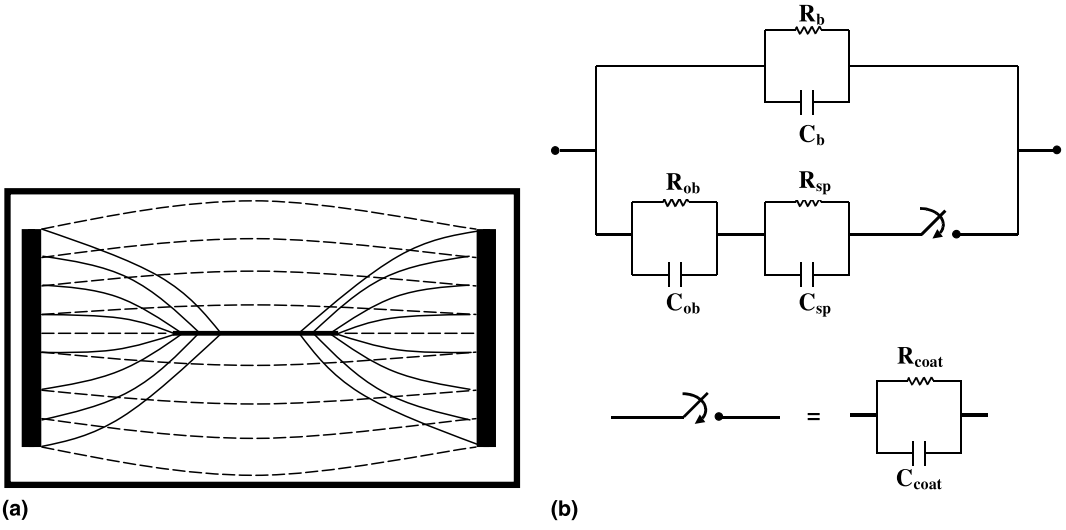

Fig. 3. (a) Current distributions at DC (dashed lines) and at the "cusp" frequency (solid lines) arising from the (b) equivalent circuit for the frequency-switchable fiber coating model. The "cusp" frequency is at the minimum $|Z_{imag}|$ between the bulk arcs with fiber(s) present in Figs. 1 and 2. (Subscript code: b = bulk, ob = outer bulk, sp = spreading, coat = coating).

medium, the spreading resistance decreases dramatically over the first 5 diameters of submersion and decreases much more gradually thereafter [3]. For example, at 5 diameters of submersion the spreading resistance is approximately 10% of the value given by Eq. (1) [3]. This suggests that most of the current flow to high aspect ratio fibers will bunch near the tips, as we showed previously [3].

The most important factor in aspect ratio is fiber length, since this governs the amount of surrounding matrix which is bypassed at the "cusp frequency" (the cusp between the two bulk arcs in Fig. 1). Fig. 4(a) shows single fiber/wire simulator results with varying lengths of carbon (graphite) wire suspended in water. In each case the wire was centered between the aluminum measuring electrodes. There is a clear shift of the cusp resistance as the length of wire increases. Since the spreading resistance is approximately the same in each case, the reduction in R_{cusp} (the resistance at the cusp) corresponds to reduction in the outer bulk contributions to the lower (fiber) current path in Fig. 3(b). A useful parameter to quantify these changes is the "gamma parameter" [2,3]:

$$\gamma = (R_{DC} - R_{cusp})/R_{DC}, \tag{2}$$

where R_{DC} is the DC resistance (with or without the fiber), and R_{cusp} has already been defined. The "gamma parameter" is a measure of the extent of bulk arc subdivision due to the presence of fibers. In Fig. 4(a), this subdivision clearly increases with the length of fiber employed. Fig. 4(b) plots the variation in γ with fiber length. Also shown are changes in γ with the number of fibers in a row (experiments described below). It is clear that fiber length (aspect ratio) has a strong influence on the impedance behavior.

3.3. Fiber volume fraction

Two simulator experiments were performed to investigate the role of fiber loading (volume fraction) on the overall composite response. The first involved approaching steel rods (6.4 mm diameter by 150 mm in length) under water in the 2000 ml graduated cylinder. Fig. 5 shows how the cusp resistance varies with the spacing between rod tips. At large spacings R_{cusp} varies linearly with distance, the slope corresponding roughly to the resistance of the right cylinder of water between their tips (whose area is that of the graduated cylinder) and the intercept corresponding to twice the spreading resistance at each rod tip. Note that spreading resistance is a significant portion of the overall resistance at the cusp frequency. As the rods approach one another there is a noticeable reduction in cusp resistance at spacings below ~3 rod diameters, as less and less of the surrounding water is involved in current flow. The inset diagram shows that the curve approaches the line corresponding to the resistance of the right cylinder of water of the same diameter as the rods and whose length was equal to the spacing between the rod tips. To calculate this line the conductivity of the tap water was measured inside a short piece of polymer tubing of known diameter. Fig. 5 suggests that R_{cusp} will vary gradually with fiber spacing until fibers come within a few radii of one another, whereupon more dramatic reductions in R_{cusp} can be anticipated.

This was borne out in a second set of simulations in the small box simulator. Beginning with a single 10 mm long fiber/wire (0.5 mm diameter) positioned axially and equidistant from the measurement electrodes 90 cm apart, additional fibers of identical length were added in a collinear fashion, but always maintaining a constant spacing from fiber-to-fiber and from fiber-to-electrode. In Fig. 4(b) the variation in gamma parameter is

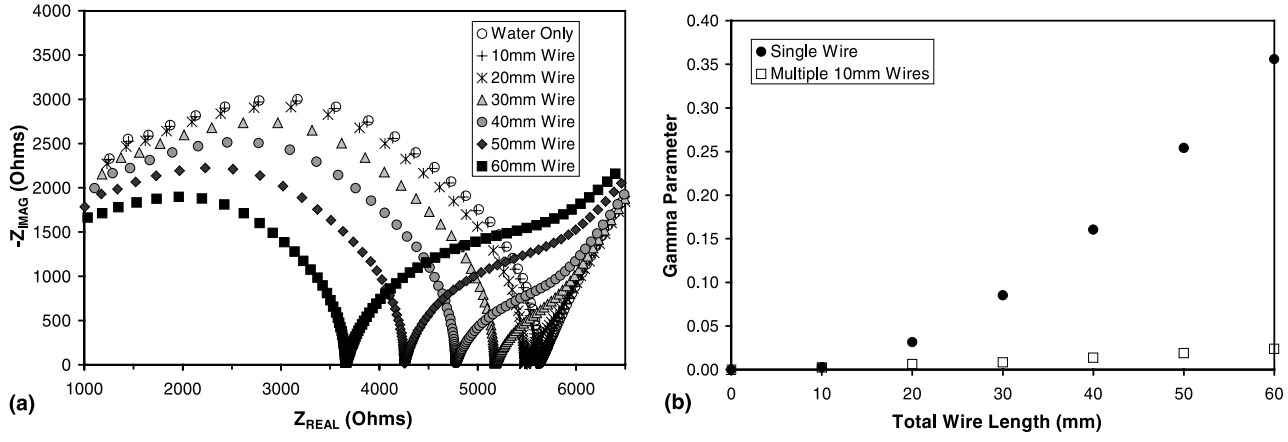

Fig. 4. (a) Nyquist plots of single graphite wires/fibers of different lengths in tap water between aluminum electrodes. (b) γ vs. length for single fibers and vs. cumulative length for equally spaced multiple fibers in collinear alignment.

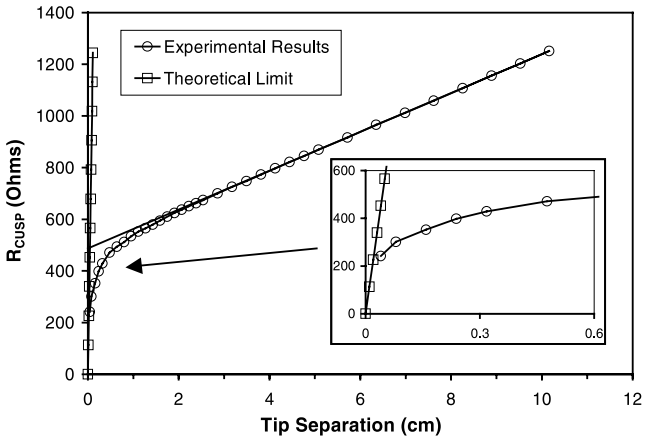

Fig. 5. Cusp resistance vs. separation between two 6.4 mm diameter, 150 mm long steel electrodes in a 2000 ml graduated cylinder of tap water. Inset diagram shows resistance at small separations.

plotted vs. overall fiber length. Although there were noticeable increases in γ, these changes were much less than for a single wire of increasing length. This is because each additional separation between adjacent wires in the collinear experiment introduces two spreading resistance contributions which, as evidenced by the intercept in Fig. 5, can be quite large. These spreading resistances tend to cancel the effect of additional wire length in the applied field direction. Unless the gap between fibers becomes quite small (e.g., of the order of the rod diameter – see Fig. 5) or adjacent fibers touch (becoming essentially one long wire), the net increase in γ (drop in R_{cusp}) will remain small.

It is instructive to compare the impedance spectra for the two composites in Fig. 1. At 1 wt% loading the volume fractions of fibers are 0.25% for the steel-reinforced composite vs. 0.88% for the carbon-reinforced composite, owing to the difference in relative densities for the fibers. As mentioned above, the final fiber length in the carbon-reinforced composite ($\sim$1 mm) is comparable to that in the steel-reinforced composite ($\sim$2 mm). This suggests that the noticeable difference in impedance behavior in Fig. 1 is primarily attributable to the difference in fiber loading. Using the geometric parameters for each system, we calculate the fiber density to be $\sim$1.7/mm^3 for the steel-reinforced composite and $\sim$35/mm^3 for the carbon-reinforced composite. These numbers indicate a much smaller fiber-to-fiber spacing for the carbon fiber system vs. the steel fiber system. The percolation threshold was also calculated based upon the "excluded volume" approach [20,21]. The values obtained were comparable, 0.71 vol% for the steel-reinforced composite and 0.85 vol% for the carbon-reinforced composite. Therefore, the steel fiber system is well below its percolation threshold, whereas the carbon system is near its percolation threshold.

Experimentally determined percolation thresholds have been reported for various fiber composites. The results are highly sensitive to the aspect ratio of the fibers employed. Bigg et al. [22] showed there was an inverse relationship between the percolation threshold and the fiber aspect ratio in carbon fiber-polymer composites; fibers with an aspect ratio of $\sim$200 gave a percolation threshold of $\sim$1 vol%. Carmona et al. [23,24] studied the percolation threshold in carbon fiber-based epoxy and elastomer composites. With an aspect ratio of 100, the percolation threshold was as low as 0.55 vol%. (The aspect ratios in the present work were 67 for the steel fibers and $\sim$56 for the carbon fibers.) In cement-based systems, Xie et al. [25] reported significantly higher percolation thresholds, e.g., 4 vol% for carbon fibers with an aspect ratio of $\sim$56 vs. 1 vol% for carbon fibers with an aspect ratio of $\sim$167. They also reported percolation thresholds of 10 vol% for steel fibers with an aspect ratio of 40 vs. 7 vol% for steel fibers with an aspect ratio of 120. The diameters of fibers in the Xie et al. [25] work were virtually identical to those in the present study. In contrast, Chung and co-workers [26,27] found virtually instantaneous reductions of DC resistivity with additions of carbon fibers (final aspect ratio unspecified) or steel fibers (aspect ratio $\sim$83) as small as 0.10 vol%. Mixing/dispersion of fibers undoubtedly plays an important role in determining actual percolation threshold, as pointed out by Chung [26].

Fig. 1 shows that the gamma parameter for the carbon fiber composite in the present study is much larger ($\sim$0.64) than for the steel fiber composite ($\sim$0.21). The reduction in the cusp resistance is consistent with higher fiber density, smaller fiber-to-fiber distances, and being closer to the percolation threshold in the carbon-reinforced cement. A systematic study of DC vs. cusp-frequency AC percolation thresholds in steel and carbon fiber-reinforced cement composites is currently being undertaken.

3.4. Fiber orientation

We showed previously that as the angle (θ) between the fiber axis and the direction of applied field is varied, the gamma factor obeys a $\cos^2\theta$ dependence [3]. The original single fiber simulator data were noisy, so this experiment was repeated in the large box simulator with a longer steel wire (81 mm, 0.5 mm diameter) and a more accurate protractor. The results are plotted in Fig. 6, and agreement with the $\cos^2\theta$ dependence is excellent.

The interpretation of Fig. 6 is straightforward. When the fiber axis is in the direction of applied field ($\theta = 0$), the entire length of the wire is available for short-circuiting the surrounding matrix at the cusp frequency; γ has its maximum value. On the other hand, when the fiber is oriented perpendicular to the applied field, only

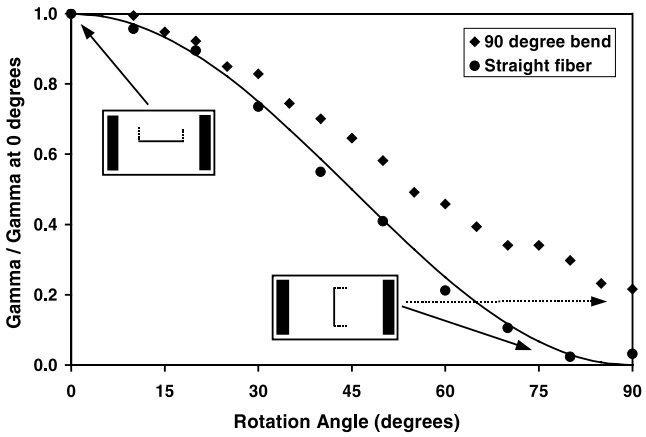

Fig. 6. Plot of $\gamma((R_{DC} - R_{cusp})/R_{DC})$ vs. the angle of orientation between a single wire or staple and the direction of applied field. The solid curve represents $\cos^2\theta$.

its diameter is available for short-circuit current flow. Since this is negligibly small, γ is essentially zero, and the Nyquist plot is virtually indistinguishable from the case with no fiber present.

This result suggests that impedance spectroscopy can be employed to test for preferred fiber orientation in composites. For example, Gerhardt [13] measured $\gamma \sim 0.35$ parallel to the hot-pressing direction, but $\gamma \sim 0.90$ perpendicular to the hot-pressing direction, in mullite-matrix/SiC whisker composites. The larger number corresponds to measuring in the direction of preferred fiber orientation. Wang et al. [14] claimed to have achieved a high degree of fiber orientation in extruded/hot-pressed Si_3N_4/SiC whisker composites. They also reported impedance spectra. As the angle between the fiber direction and the direction of applied field increased from $\theta = 0°$ (parallel) to $\theta = 90°$ (perpendicular), γ decreased from 0.85 to essentially zero. Based upon the present work, we would concur that a high degree of fiber orientation had been achieved in these specimens. Finally, Torrents et al. [3] made extruded specimens of carbon fiber-reinforced OPC composites and measured impedance spectra in various directions. They found γ to increase from 0.4 perpendicular to the extrusion direction ($\theta = 90°$) to approximately 0.8 at an angle of $\theta = 18°$. The relatively large value measured perpendicular to the extrusion direction, in a direction supposedly perpendicular to the fibers, indicates that the orientation was far from perfect in this study. An implication of this result is that the gamma parameter may also be used to assess the degree of fiber orientation in actual composites.

3.5. Fiber shape

Naaman [28] has catalogued a range of fiber shapes for cement-based composites. These include dumbbell and hooked-end fibers, designed to improve anchorage and/or work of pullout during mechanical deformation. The presence of end units, whether dumbbells or hooks, can also significantly reduce the spreading resistance of fibers/wires in impedance measurements. The large chamber single-fiber simulator was used to investigate end shape effects on the resulting impedance spectra. Three "fibers" of identical length (81 mm) were employed – straight (0.5 mm diameter), hooked-end (staple-shaped, with 19 mm long segments bent 90° to the 81 mm long fiber spine), and a dumbbell (with 19 mm diameter disks, 0.5 mm thick, at each end of the 81 mm long fiber spine). Impedance spectra were taken with the fibers submerged in water equidistant from the measuring electrodes. From the resulting spectra the corresponding gamma parameters were calculated using Eq. (2). In Table 1 the values have been normalized by the value of γ for the straight wire aligned parallel to the applied field.

Table 1
Gamma parameters for different fiber shapes

Measured gamma parameters vs. field alignment (normalized to the straight fiber in parallel alignment to the applied field)		
Fiber	Parallel	Perpendicular
Straight	1.00	<0.01
90° Hooked-end	2.58	0.20, <0.01*
Dumbbell-shaped	3.75	0.31

*The second value is with the plane of the fiber perpendicular to the applied field; the first value is with the end sections pointing at one electrode.

In the field-parallel direction, the hooked-end and dumbbell-shaped fibers show significant increases in γ over the straight fiber. This is reasonable since the increased area of the fiber ends results in a greatly reduced spreading resistance. More importantly, in the field-perpendicular direction, the hooked-end and dumbbell fibers can exhibit substantial gamma factors whereas the straight fiber does not. As described above, the straight fiber becomes essentially "invisible" when positioned perpendicular to the applied field. In contrast, dumbbell-shaped fibers will never be "invisible" while hooked-end fibers will be "invisible" only when the plane of the fiber is perpendicular to the field direction. If instead the ends are pointed in the direction of applied field, some degree of arc subdivision will be observed. This can be seen in the gamma parameter vs. rotation angle plot of Fig. 6, where the hooked-end fiber/wire positioned with its ends in the direction of applied field (rotation angle of 90°) exhibits a non-zero value of gamma (see Table 1). Studies of composites with fibers of various shapes are underway to investigate fiber shape/orientation effects in actual composites.

4. Conclusions

Ordinary portland cement-based composites with 1 wt% of short (1–2 mm) steel or carbon fibers were found to exhibit two bulk arcs in Nyquist plots of impedance data. This is in contrast with a single bulk arc for the cement paste alone. There were negligible changes in DC resistance with the addition of fibers. The "cusp" resistance, at the intersection of the two bulk arcs, was different for the two composite systems.

A "frequency-switchable fiber coating" model can account for both the dual-arc impedance behavior and the negligible shift in DC resistance upon the addition of fibers. A highly resistive passive oxide film (on steel) or a polarization layer/double layer (on carbon) effectively insulates the fibers at DC or low AC frequencies. As frequency is raised, however, displacement currents through the thin "coating" capacitance short out the coating, and the fibers become short-circuits for current flow at the "cusp" frequency.

Several factors govern the impedance response, especially the cusp resistance, of composites. A "gamma factor", or ratio of the difference in DC and cusp resistances to the DC resistance, is useful for characterizing the microstructure–electrical property relationships in composites. Fiber aspect ratio, or fiber length at fixed diameter, plays a dominant role. Longer fibers allow current to bypass more of the surrounding matrix at the cusp frequency. Fiber loading (volume fraction) is also important. As two fibers approach one another end-to-end, cusp resistance decreases linearly (matrix effect) and then drops rapidly when their tips are within a few fiber radii of each other. In the present study, the shorter fiber-to-fiber distances in the carbon fiber-reinforced OPC vs. the steel fiber-reinforced OPC resulted in a larger gamma factor (and a lower cusp resistance).

Impedance spectra are also sensitive to fiber orientation and shape effects. When field is applied in the direction of the fibers (in an oriented system) a maximum gamma factor will be obtained. In contrast, when field is applied perpendicular to the direction of the fibers, they will be effectively "invisible" in the impedance spectrum, i.e., no second bulk arc (or a zero gamma factor). The addition of hooked ends or dumbbell ends on fibers greatly reduces the spreading resistance (and increases gamma) when field is applied along the fiber axis. When field is applied perpendicular to the fiber axis, bulk arc subdivision can still be present due to the hooked ends or dumbbells being aligned with the field. These results suggest that impedance spectroscopy may be useful for characterizing oriented composites (full or partial alignment) and also those involving fibers with unusual shapes.

Acknowledgements

This work was supported in part by the National Science Foundation Science and Technology Center for Advanced Cement-Based Materials under grant no. CHE-91-20002 and by the National Science Foundation under grant no. DMR-00-73197.

References

[1] Evans AG. Perspective on the development of high-toughness ceramics. J Am Ceram Soc 1990;73(12):187–206.
[2] Torrents JM, Mason TO, Garboczi EJ. Impedance spectra of fiber-reinforced cement-based composites: a modeling approach. Cem Concr Res 2000;30:585–92.
[3] Torrents JM, Mason TO, Peled A, Shah SP, Garboczi EJ. Analysis of the impedance spectra of short conductive fiber-reinforced composites. J Mater Sci 2001;36:4003–12.
[4] Test method for fiber content of unidirectional fiber-resin composites by electrical resistivity, ASTM D 790-84a (1980), discontinued 1988.
[5] Muto N, Yanagida H, Nakatsuji T, Sugita M, Ohtsuka Y. Preventing fatal fractures in carbon-fiber–glass-fiber-reinforced plastic composites by monitoring change in electrical resistance. J Am Ceram Soc 1993;76(4):875–9.
[6] Wang X, Chung DDL. Real-time monitoring of fatigue damage and dynamic strain in carbon fiber-polymer matrix composite by electrical resistance measurement. Smart Mater Struct 1997;6:504–8.
[7] Chung DDL. Self-monitoring structural materials. Mater Sci Eng R 1998;22:57–78.
[8] Wang X, Chung DDL. Short carbon fiber reinforced epoxy coating as a piezoresistive strain sensor for cement mortar. Sensors Actuators A 1998;71:208–12.
[9] Wang S, Chung DDL. Self-monitoring of strain in silicon carbide whisker reinforced silicon nitride. Smart Mater Struct 1997;6:199–203.
[10] Chen P-W, Chung DDL. Carbon-fiber-reinforced concrete as an intrinsically smart concrete for damage assessment during dynamic loading. J Am Ceram Soc 1995;78(3):816–8.
[11] Chen P-W, Chung DDL. Carbon fiber reinforced concrete as an intrinsically smart concrete for damage assessment during static and dynamic loading. ACI Mater J 1996;93:341–50.
[12] Gu P, Xu Z, Xie P, Beaudoin JJ. An a.c. impedance spectroscopy study of micro-cracking in cement-based composites during compressive loading. Cem Concr Res 1993;23:675–82.
[13] Gerhardt R. Microstructural characterization of composites via electrical measurements. Proc Ceram Eng Sci 1994:1174–81.
[14] Wang C-A, Huang Y, Li Y, Zhang Z. Complex impedance analysis on orientation effect of whiskers in oriented SiC(w)/Si_3N_4 composites. J Am Ceram Soc 2000;83(11):2689–92.
[15] Ford SJ, Shane JD, Mason TO. Assignment of features in impedance spectra of the cement-paste/steel system. Cem Concr Res 1998;28(12):1737–51.
[16] Peled A, Torrents JM, Mason TO, Shah SP, Garboczi EJ. Electrical impedance spectra to monitor damage during tensile loading of cement composites. ACI Mater J 2001;98:313–22.
[17] Boukamp A. Equivalent circuit (EQUIVCRT.PAS). Department of Chemical Engineering, University of Twente, The Netherlands, 1990.

[18] Sohn D, Mason TO. Electrically induced microstructural changes in portland cement pastes. Adv Cem Based Mater 1998;7:81–8.
[19] Newman J. Resistance for flow of current to a disk. J Electrochem Soc 1966;113:501–2.
[20] Balberg I, Anderson CH, Alexander S, Wagner N. Excluded volume and its relation to the onset of percolation. Phys Rev B 1984;30(7):3933–43.
[21] Yi JY, Choi GM. Percolation behavior of conductor–insulator composites with varying aspect ratio of conductive fiber. J Electroceramics 1999;3(4):361–9.
[22] Bigg DM, Stutz DE. Plastic composites for electromagnetic-interference shielding applications. Polym Comp 1983;4(1):40–6.
[23] Carmona F, Conet R, Delhaes P. Piezoresistivity of heterogeneous solids. J Appl Phys 1987;61:2550–7.
[24] Carmona F, Barreau P, Delhaes P, Conet R. Experimental model for studying the effect of anisotropy and percolation conduction. J Phys Lett 1980;41:L531–4.
[25] Xie P, Gu P, Beaudoin JJ. Electrical percolation phenomena in cement composites containing conductive fibres. J Mater Sci 1996;31:4093–7.
[26] Chen P-W, Chung DDL. Improving the electrical conductivity of composites comprised of short conducting fibers in a nonconducting matrix: the addition of a nonconducting particulate filler. J Electr Mat 1995;24(1):47–51.
[27] Wen S, Chung DDL. Seebeck effect in steel fiber reinforced cement. Cem Concr Res 2000;30:661–4.
[28] Naaman AE. New fiber technology. ACI Concr Int 1998;20(7): 57–62.